PERGAMON

International Journal of Heat and Mass Transfer 43 (2000) 677–686

International Journal of HEAT and MASS TRANSFER

www.elsevier.com/locate/ijhmt

The effect of free-floating dendrites and convection on macrosegregation in direct chill cast aluminum alloys Part I: model development

Christopher J. Vreeman[a,*], Matthew John M. Krane[b], Frank P. Incropera[c]

[a]*Heat Transfer Laboratory, School of Mechanical Engineering, Purdue University, West Lafayette, IN 47907, USA*
[b]*School of Materials Engineering, Purdue University, West Lafayette, IN 47907, USA*
[c]*College of Engineering, University of Notre Dame, Notre Dame, IN 46556, USA*

Received 26 June 1998; received in revised form 18 May 1999

Abstract

To obtain a better understanding of the evolution of macrosegregation during the direct chill casting of aluminum alloys, a binary mixture model has been developed that accounts for the redistribution of alloying elements through the transport of free-floating dendrites and fluid flow in the melt and mushy zones of a solidifying ingot. Separate and distinct mixture momentum equations are employed to account for momentum transfer in two-phase regions which include a slurry of free-floating dendrites and a rigid solid matrix. A scaling analysis revealed that the flow of liquid and free-floating dendrites is controlled by a balance between buoyancy forces arising from mixture density variations and the development of an adverse pressure gradient. In a companion paper, the model is used to predict macrosegregation in Al–4.5 wt% Cu and Al–6.0 wt% Mg billets.

Keywords: Heat transfer; Continuous casting; Direct chill casting; Macrosegregation; Fluid flow; Shrinkage; Solidification; Aluminium alloys; Semi-continuous casting; Equiaxed dendrites; Thermosolutal buoyancy; Natural convection; Binary alloys

1. Introduction

Casting defects arising during the solidification of metal alloys impose constraints upon many casting processes, which contribute significantly to the cost of manufacturing metal alloy products. A particular problem that occurs in a wide range of casting processes, including the direct chill (DC) casting of aluminum alloys, is the uncontrolled redistribution of alloying elements during solidification, which leads to large-scale composition inhomogeneities, commonly referred to as macrosegregation. Macrosegregation in DC cast ingots produces non-uniform mechanical properties [1], significantly impacts structural homogeneity in the finished product [2], and seriously constrains the size, alloy composition, and rate at which ingots may be produced [3].

Direct chill casting is a semi-continuous process in which molten aluminum enters the top of a water-cooled mold, while a solid ingot is drawn from below

* Corresponding author. Present address: Rocketdyne Propulsion and Power, 6633 Canoga Avenue MS PA84, Canoga Park, CA 91309-7922, USA. Tel.: +1 818 586 1156; fax: +1 818 586 0159.

E-mail address: christophe.j.vreeman@boeing.com (C.J. Vreeman).

0017-9310/99/$ - see front matter
PII: S0017-9310(99)00174-X

Nomenclature

B	specific buoyancy force (m/s^2)
c	specific heat (J/kg K)
d	characteristic dendrite diameter (μm)
D	mass diffusion coefficient (m^2/s)
f	mass fraction
F	dimensionless composition
Fr_R	slurry region Froude number, $v_0/\sqrt{Rg}$
g	volume fraction; gravitational acceleration (m/s^2)
h	enthalpy (J/kg)
k	thermal conductivity (W/m K)
k_p	equilibrium partition coefficient
K	permeability (m^2)
p	pressure (N/m^2)
P	reduced pressure (N/m^2)
r, z	axisymmetric coordinates (m)
R	billet radius (m)
Re_R	slurry region Reynolds number, $\rho_l v_0 R/\mu_l$
t	time (s)
T	temperature (K)
u	axial velocity component (m/s)
v	radial velocity component (m/s)
$\vec{V}$	velocity vector (m/s)
β	contraction ratio
β_S	solutal expansion coefficient
β_T	thermal expansion coefficient (1/K)
ε	limit of integration
η_s	dimensionless solid–liquid viscosity ratio, $\bar{\mu}_s/\mu_l$
θ	dimensionless temperature
μ	dynamic viscosity (kg/s m)
ρ	density (kg/m^3)

Subscripts

i	mold inlet condition
l	liquid
liq	liquidus
m	mixture
0	reference, nominal value
p	packed, rigid structure
s	solid
S	solutal
SH	superheat
T	thermal

Superscript

A	generic element in a binary mixture

(Fig. 1). The molten aluminum begins to solidify as it comes into contact with the mold wall, forming a thin solid layer around a liquid melt, commonly referred to as the sump. As the ingot is withdrawn from the bottom of the mold, water jets impinge on the surface, directly cooling and completely solidifying the ingot.

A commonly observed, surface-to-surface distribution of alloying elements at a transverse cross-section of a DC cast ingot is shown in Fig. 1, revealing distinct regions of positive (solute-rich) and negative (solute-depleted) segregation [3]. The subsurface enrichment near the ingot surface is attributed to a combination of shrinkage induced flow of solute-rich liquid toward the mold wall, where solidification rates are highest, and exudation induced by local remelting of the ingot surface as the solid shell pulls away from the mold. Once a structurally sound ingot surface has formed and solidification rates have decreased, more normal segregation behavior is observed, with the solute composition increasing with decreasing radius from the solute-depleted region near the ingot surface. While this trend may be expected to continue, ingots produced by DC casting often exhibit a significant decrease in solute composition near the centerline (Fig. 1).

Experimental studies have provided some insight into the mechanisms that control macrosegregation in DC cast ingots, especially at the centerline. Yu and Granger [3] investigated negative segregation in Al–Cu–Mg slabs and found that negative segregation of copper and magnesium at the centerline was accompanied by a duplex microstructure consisting of adjacent large and fine equiaxed grains. Measurements across a single large grain with an electron microprobe revealed that, away from the grain boundary, the grain was uniformly copper-depleted. As a result, Yu and Granger concluded that the duplex microstructure at the centerline of DC cast ingots and the accompanying negative segregation resulted from the settling of solute-depleted, free-floating dendrites that formed near the top of the sump and were subsequently swept to the bottom of the sump by convection currents in the melt. This theory was also supported by significant positive titanium segregation at the centerline [3], which is present in grain refining particles that serve as nucleation sites for free-floating dendrites. Duplex microstructures accompanied by the negative centerline segregation have also been observed by Chu and Jacoby [2] and Dorward and Beerntsen [4], and negative centerline segregation with positive segregation of

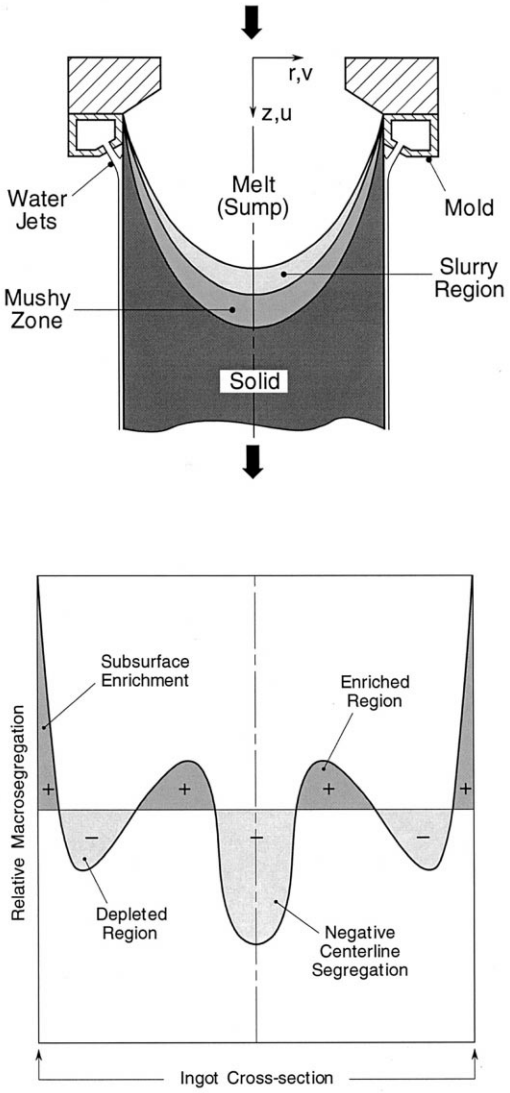

Fig. 1. Direct chill casting process and commonly observed surface-to-surface distribution of alloying elements in DC cast ingots.

titanium was observed in ingots cast by Gariepy and Caron [5].

In contrast to the foregoing studies, Finn et al. [1], in observing the effect of grain refiner additions on macrosegregation in DC cast Al–4.5 wt% Cu billets, found a duplex microstructure accompanied by positive copper segregation at the centerline of a billet. Furthermore, in a billet cast without a grain refiner, they observed negative segregation without the duplex microstructure. While Finn et al. agreed that duplex microstructures at the centerline result from the transport of free-floating dendrites, they suggested that the equiaxed mushy zone in their grain-refined billet must have been permeable enough to allow a high degree of solute-rich interdendritic liquid to flow toward the centerline, thereby overcoming the influence of solute-depleted dendrites settling at the bottom of the sump.

In recent years, so-called surface segregation models [6–8] that employ one-dimensional transport equations to account for interdendritic fluid flow have been used to model macrosegregation and exudation near the surface of DC cast ingots and have predicted surface enrichment and regions of solute depletion. Furthermore, Mo et al. [7] found good agreement between calculated and experimentally observed compositions in the exudation layer.

Of particular interest in modeling macrosegregation during DC casting are single domain models that implicitly couple transport phenomena in the melt, mushy zone, and solid regions of a solidifying ingot, thereby eliminating the need to model each region independently. Reviews of related literature have been published [9,10].

Flood et al. [11] were the first to apply a single domain model to predict macrosegregation in DC cast Al-4.5 wt% Cu billets by using volume-averaged, mixture equations to account for mass, momentum, energy, and species conservation. They assumed that the mushy zone consisted of a rigid, permeable dendritic matrix with the solid moving at the casting speed, thus neglecting the influence of free-floating dendrites, and predicted negative segregation of copper from the surface to a distance of approximately 10 cm from the billet centerline. Within the centerline region, positive segregation was predicted, and the copper composition increased dramatically as the radius approached zero. Though Flood et al. predicted negative segregation just within the billet surface, as is commonly observed (Fig. 1), the level of macrosegregation predicted at the centerline was much higher than that observed in experimental studies [1–5].

The first use of a single domain model of the DC casting process which includes the influence of free-floating dendrites is attributed to Reddy and Beckermann [12], who employed a modified version of the two-phase model developed by Ni and Beckermann [13] to simulate the DC casting of two Al–4.5 wt% Cu billets. In both cases, the boundary conditions simulated the experimental conditions of Finn et al. [1]. In one case, the solid phase was assumed to form a rigid structure moving at the casting speed. In the other case, the transport of solute-depleted, free-floating dendrites was modeled by using an interfacial drag correlation that varied between Stokes Law for a single sphere and the Kozeny–Carman permeability model for a packed bed of spheres, with the solid phase assumed to form a rigid structure at a solid volume fraction of 0.637. In addition to modeling heat, mass, momentum, and species

transfer, Reddy and Beckermann employed a grain transport equation to calculate the local grain density, with the assumption that grains were not generated by nucleation or fragmentation and did not disappear due to remelting.

In the simulation with no free-floating solid, Reddy and Beckermann [12] predicted subsurface enrichment, followed by a narrow depleted region just within the surface. From this region to the centerline, varying positive and negative segregation was predicted with positive segregation ultimately occurring at the centerline and attributed to the buoyancy driven flow of copper-rich liquid to the bottom of the sump. In the simulation with free-floating dendrites, they predicted positive segregation near the surface, but did not predict the near-surface depleted region. Significant negative segregation was, however, predicted at the centerline, which Reddy and Beckermann attributed to the advection of copper-depleted dendrites to the bottom of the sump. Both cases lacked consistent agreement of the predicted macrosegregation distribution with the experimental data of Finn et al. [1], and the connection between the transport of free-floating dendrites and absence of a near-surface depleted region (Fig. 1) was not addressed. However, Reddy and Beckermann were the first to include the transport of free-floating dendrites into a fully coupled, single domain, macrosegregation model of the DC casting process and to predict the resulting negative segregation at the centerline.

More recently, Reddy and Beckermann [14] conducted further DC casting simulations of Al-4.5 wt% Cu billets to examine the effect of the grain density and interdendritic fluid flow on macrosegregation in billets devoid of free-floating dendrites. With a low grain density, they predicted the commonly observed subsurface enrichment and depleted regions, as well as positive segregation at the centerline due to the buoyancy driven flow of copper-rich liquid in the melt and mushy zone to the bottom of the sump. With a higher grain density, they found that buoyancy driven interdendritic fluid flow toward the centerline was effectively restricted, causing flow in the mushy zone to be driven primarily by shrinkage toward the solidus, and therefore, away from the centerline. Consequently, negative segregation was predicted at the centerline. Additionally, predictions for the high grain density were in good agreement with the experimental results of Finn et al. [1] for their non-grain refined billet. Therefore, Reddy and Beckermann [14] demonstrated that, if the mushy zone consists of a rigid dendritic structure without free-floating dendrites, its permeability significantly influences macrosegregation in DC cast billets.

The objective of the current study is to develop a fully coupled, single-domain, mixture model of the DC casting process that simultaneously accounts for the redistribution of alloying elements by the transport of free-floating dendrites and fluid flow in the melt and mushy zone. In a companion paper [15], the newly proposed mixture model is used to simulate macrosegregation in Al-4.5 wt% Cu and Al-6.0 wt% Mg billets. By conducting these simulations, the manner in which segregation develops, as well as its dependence on specific transport phenomena, may be clearly established and physical phenomena that may require further modeling are identified [15].

2. Model equations

The continuum mixture model originally formulated by Bennon and Incropera [16] and clarified by Prescott et al. [17] is used as a starting point for the current single domain, mixture model of macrosegregation in DC cast ingots. For a cylindrical billet and axisymmetric casting conditions, the continuum mixture equations are of the form:

$$\frac{\partial \rho}{\partial t} + \nabla \cdot \left(\rho \vec{V}\right) = 0 \tag{1}$$

$$\frac{\partial}{\partial t}(\rho u) + \nabla \cdot \left(\rho \vec{V} u\right) = \nabla \cdot \left(\mu_l \frac{\rho}{\rho_l} \nabla u\right) - \frac{\mu_l}{K_z}\frac{\rho}{\rho_l}(u - u_s) - \rho_l g\Big[\beta_{T,l}(T - T_0) + \beta_{S,l}\left(f_l^{A} - f_0^{A}\right)\Big] - \frac{\partial P}{\partial z} \tag{2}$$

$$\frac{\partial}{\partial t}(\rho v) + \nabla \cdot \left(\rho \vec{V} v\right) = \nabla \cdot \left(\mu_l \frac{\rho}{\rho_l} \nabla v\right) - \frac{\mu_l}{K_r}\frac{\rho}{\rho_l} v - \mu_l \frac{\rho}{\rho_l}\frac{v}{r^2} - \frac{\partial P}{\partial r} \tag{3}$$

$$\frac{\partial}{\partial t}(\rho h) + \nabla.\left(\rho \vec{V} h\right) = \nabla \cdot \left(\frac{k}{c_s} \nabla h\right) + \nabla \cdot \left(\frac{k}{c_s} \nabla (h_s - h)\right) - \nabla \cdot \left(\rho\left(\vec{V} - \vec{V}_s\right)(h_l - h)\right) \tag{4}$$

$$\frac{\partial}{\partial t}\left(\rho f^{A}\right) + \nabla \cdot \left(\rho \vec{V} f^{A}\right) = \nabla \cdot \left(\rho f_l D_l^{A} \nabla f^{A}\right) + \nabla \cdot \left(\rho f_l D_l^{A} \nabla\left(f_l^{A} - f^{A}\right)\right) - \nabla \cdot \left(\rho\left(\vec{V} - \vec{V}_s\right)\left(f_l^{A} - f^{A}\right)\right) \tag{5}$$

The mixture momentum Eqs. (2) and (3) were derived by assuming that the mushy zone consists of a rigid, dendritic matrix which moves at a prescribed velocity and is saturated by interdendritic liquid. For the axi-

symmetric billet (Fig. 1), the radial solid velocity component, v_s, of the rigid dendritic structure is zero, while the axial solid velocity component, u_s, corresponds to the casting speed. Other assumptions, made in the development of Eqs. (4) and (5), include local thermal equilibrium between the solid and liquid ($T = T_s = T_l$) and negligible species diffusion in the solid relative to the liquid ($D_l^B \gg D_s^B$).

More recently, Ni and Incropera [18,19] developed single-domain mixture momentum equations for two-phase regions consisting of a slurry of free-floating dendrites by summing solid and liquid momentum equations previously developed by Ni and Beckermann [13]. Assuming that the average solid and liquid interfacial velocities are equal to the free-floating dendrite velocity, the equations developed by Ni and Incropera [18] take the following form in the axial direction of the axisymmetric coordinate system:

$$\begin{aligned}\frac{\partial}{\partial t}(\rho u) + \nabla\cdot\left(\rho\vec{V}u\right) &= \nabla\cdot\left(\mu_l\frac{\rho}{\rho_l}\nabla u\right)\\ &+ \nabla\cdot\left(\mu_l u\nabla\left(\frac{\rho}{\rho_l}\right)\right) - \nabla\cdot\left(\mu_l\frac{\rho f_s}{\rho_l}\nabla u_s\right)\\ &- \nabla\cdot\left(\mu_l u_s\nabla\left(\frac{\rho f_s}{\rho_l}\right)\right) + \nabla\cdot(\mu_l u_s\nabla g_s)\\ &+ \nabla\cdot(\mu_s g_s\nabla u_s) - \nabla\cdot\left[\left(\frac{\rho f_s}{f_l}\right)\left(\vec{V}-\vec{V}_s\right)(u-u_s)\right]\\ &+ \rho B_z - \frac{\partial p}{\partial z}\end{aligned} \tag{6}$$

In Eq. (6), a mixture viscosity formulation for a solid–liquid slurry ($\mu_m = \mu_l(1 - g_s/g_{s,p})^{-2.5g_{s,p}}$) [20] was separated into individual liquid and solid viscosity contributions (μ_l and $\mu_s = (\mu_m - g_l\mu_l)/g_s$) and used to account for the mixture viscous momentum exchange. Interactions between free-floating dendrites were assumed to increase with increasing solid fraction, up to a critical packing fraction, $g_{s,p}$, where the solid dendrites coalesce to form a rigid structure (i.e., $\mu_s \to \infty$ as $g_s \to g_{s,p}$) [18]. The solid velocity of free-floating dendrites was related to the liquid velocity by the following expression [19],

$$\vec{V}_s - \vec{V}_l = \frac{(1-g_s)}{18\mu_m}(\rho_s - \rho_l)d^2\vec{g}, \tag{7}$$

where d is a characteristic diameter of the free-floating dendrites and μ_m is the aforementioned mixture viscosity [18]. While Eq. (7) was derived from Stokes Law for a single spherical particle and does not account for multi-particle effects, it is used in the current study to approximate solid–liquid velocity differences, thereby providing for the settling of free-floating dendrites.

With experimental investigations suggesting that both the transport of free-floating dendrites and interdendritic fluid flow in the mushy zone contribute significantly to macrosegregation in DC cast ingots, the momentum Eqs. (2) and (3) for a rigid dendritic structure and the momentum equations [18] for a slurry of free-floating dendrites are used concurrently to model momentum transport during solidification in DC cast billets. Use of both momentum transport models is accomplished by assuming that the two-phase region in DC cast billets consists of a slurry of free-floating dendrites if the solid volume fraction is less than the designated packing fraction ($g_s < g_{s,p}$) and a rigid mushy zone consisting of packed dendrites and interdendritic liquid if $g_s \geq g_{s,p}$. Implementation then requires that momentum equations for a slurry of free-floating dendrites be applied in both the liquid and slurry regions ($0 \leq g_s < g_{s,p}$), while momentum Eqs. (2) and (3) are applied to the rigid mushy zone and the solid region ($g_{s,p} \leq g_s \leq 1$). In general, the packing fraction is not explicitly known and is related to the size and surface morphology of individual free-floating dendrites, which may vary within a particular system depending on local morphological, thermodynamic, and fluid flow conditions. In the numerical study of the companion paper [15], the packing fraction is varied from zero (no free-floating dendrites) to a maximum value of 30%, in order to determine its influence on macrosegregation.

In the current model, it is assumed that the contribution of solid dendrite interactions to macroscopic viscous momentum transfer increases with increasing solid volume fraction in the slurry region, but remains finite as $g_s \to g_{s,p}$. Furthermore, it is assumed that free-floating dendrites coming into contact with the rigid mushy zone become attached and instantaneously assume the velocity of the rigid dendritic structure through direct application of momentum Eqs. (2) and (3) when $g_s \geq g_{s,p}$. However, with this approach, the mixture (and consequently solid) viscosity model recommended by Ni and Incropera [18], which simulates an increasingly viscous slurry by increasing to infinite values as the solid volume fraction approaches the packing fraction, cannot be used. To retain relative phase motion associated with dendrite settling and interdendritic fluid flow at the discrete interface between the slurry and the rigid mushy zones ($g_s = g_{s,p}$), the mixture and solid viscosities are instead represented by fixed values obtained by evaluating the integrated averaged of μ_m and μ_s across some finite portion of the slurry region (i.e., the integrated average from $g_s = 0$ to $g_s = \varepsilon g_{s,p}$, where $0 < \varepsilon < 1$) [15]. By using averaged mixture and solid viscosities in the slurry momentum equations and Eq. (7), relative phase motion is not artificially forced to zero as $g_s \to g_{s,p}$. The effect of using averaged viscosities on macroscopic momentum transport in the slurry region is addressed

in the subsequent scaling analysis of the slurry momentum equations in Section 3.

Since the body force term in the slurry momentum Eq. (6) involves the mixture density, rather than the liquid density appearing in Eq. (2), the term takes on a different form when the Boussinesq approximation is invoked. Employing the definition of reduced pressure ($P = p - \rho_l g z$), the following expression is obtained for the body force and pressure gradient terms appearing in Eq. (6):

$$\rho B_z - \frac{\partial p}{\partial z} = g_s(\rho_s - \rho_l)g - g_s\rho_s g\Big[\beta_{T,s}(T - T_0) + \beta_{S,s}\big(f_s^A - f_0^A\big)\Big] - g_l\rho_l g\Big[\beta_{T,l}(T - T_0) + \beta_{S,l}\big(f_l^A - f_0^A\big)\Big] - \frac{\partial P}{\partial z} \quad (8)$$

The first term on the right side of Eq. (8) represents body forces due to solid and liquid density differences, while the second and third terms represent body forces due to thermally and solutally induced density variations within the solid and liquid phases, respectively.

Substituting Eq. (8) into Eq. (6) and using the averaged solid viscosity, $\bar{\mu}_s$, the following expression is obtained for momentum transfer in the axial direction of the axisymmetric coordinate system:

$$\begin{aligned}\frac{\partial}{\partial t}(\rho u) + \nabla\cdot\left(\rho\vec{V}u\right) &= \nabla\cdot\left(\mu_l\frac{\rho}{\rho_l}\nabla u\right) + \nabla\cdot\left(\mu_l u\nabla\left(\frac{\rho}{\rho_l}\right)\right) - \nabla\cdot\left(\mu_l\frac{\rho f_s}{\rho_l}\nabla u_s\right) \\ &- \nabla\cdot\left(\mu_l u_s\nabla\left(\frac{\rho f_s}{\rho_l}\right)\right) + \nabla\cdot(\mu_l u_s\nabla g_s) \\ &+ \nabla\cdot(\bar{\mu}_s g_s\nabla u_s) - \nabla\cdot\left[\left(\frac{\rho f_s}{f_l}\right)\big(\vec{V} - \vec{V}_s\big)(u - u_s)\right] \\ &+ g_s(\rho_s - \rho_l)g - g_s\rho_s g\Big[\beta_{T,s}(T - T_0) + \beta_{S,s}\big(f_s^A - f_0^A\big)\Big] \\ &- g_l\rho_l g\Big[\beta_{T,l}(T - T_0) + \beta_{S,l}\big(f_l^A - f_0^A\big)\Big] - \frac{\partial P}{\partial z} \end{aligned} \quad (9)$$

Likewise, the radial momentum equation for the slurry region is expressed as

$$\begin{aligned}\frac{\partial}{\partial t}(\rho v) + \nabla\cdot\left(\rho\vec{V}v\right) &= \nabla\cdot\left(\mu_l\frac{\rho}{\rho_l}\nabla v\right) - \mu_l\frac{\rho}{\rho_l}\frac{v}{r^2} + \nabla\cdot\left(\mu_l v\nabla\left(\frac{\rho}{\rho_l}\right)\right) \\ &- \nabla\cdot\left(\mu_l\frac{\rho f_s}{\rho_l}\nabla v\right) + \mu_l\frac{\rho f_s}{\rho_l}\frac{v}{r^2} \\ &- \nabla\cdot\left(\mu_l v\nabla\left(\frac{\rho f_s}{\rho_l}\right)\right) + \nabla\cdot(\mu_l v\nabla g_s) \\ &+ \nabla\cdot(\bar{\mu}_s g_s\nabla v) - \bar{\mu}_s g_s\frac{v}{r^2} - \frac{\partial P}{\partial r}\end{aligned} \quad (10)$$

where $v = v_s = v_l$ from Eq. (7).

In summary, a coherent, single domain model of momentum transfer in a DC cast billet which simultaneously accounts for the transport of free-floating dendrites and interdendritic fluid flow is obtained by applying Eqs. (9) and (10) when the local solid volume fraction is less than the packing fraction ($0 \le g_s < g_{s,p}$) and applying Eqs. (2) and (3) when the local solid volume fraction is greater than or equal to the packing fraction ($g_{s,p} \le g_s \le 1$). Eqs. (1), (4) and (5) are applied throughout the computational domain, thus completing the required set of transport equations. Finally, thermodynamic equilibrium is assumed on the scale of a control volume so that diffusion is complete in the solid (lever law) and microsegregation is neglected. The method of Bennon and Incropera [21,22] is used to determine phase fractions, compositions, and temperatures, wherein the mixture enthalpy, h, and composition, f^A are used with the equilibrium phase diagram, thus providing closure for the system of equations.

3. Scaling analysis of momentum transport in the slurry region

The momentum Eqs. (9) and (10) for a slurry of free-floating dendrites may be scaled with the continuity Eq. (1) to identify dominant mechanisms for transporting free-floating dendrites to the bottom of the sump. Furthermore, by identifying terms that have a negligible impact on macroscopic momentum transport, implementation of the slurry momentum equations in a standard numerical algorithm is simplified.

Krane and Incropera [23] used a scaling analysis for unidirectional solidification of a binary alloy to confirm that Darcy's law could be used to approximate momentum transfer in mushy zones consisting of a rigid dendritic matrix, except near the liquidus where solid volume fractions are low. They also developed scaling laws for the mushy zone thickness and confirmed that fluid advection is the dominant mechanism for solutal transport and, therefore, macrosegregation during solidification.

More recently, Reese [24] derived scaling relationships to evaluate liquid velocities and temperature stratification in the sumps of DC cast ingots. Originally, Davidson and Flood [25] integrated the liquid momentum equations about a streamline and determined that fluid flow in the melt of a DC cast ingot is best characterized by a thermally driven recirculation with downward motion along the solidification front toward the centerline and upflow at the ingot center into a relatively quiescent sump. They further concluded that the thermal boundary layer in the low Prandtl number liquid adjacent to the solidifi-

cation front is much larger than the accompanying viscous boundary layer and that flow along this front is controlled by temperature gradients except in close proximity to the solid interface. Reese [24] extended the analysis by developing scaling relations for thermal boundary layer thicknesses and liquid metal velocities near the solidification front, as well as for the depth of thermal stratification in the sump. Reese further demonstrated that the fundamental nature of liquid flow in the sump of DC cast ingots is not significantly altered by the manner in which liquid enters the mold.

The scaling analysis of this study focuses on that portion of the slurry region near the interface with the rigid dendritic structure ($g_s = g_{s,p}$), where free-floating dendrites are advected by buoyancy forces along the ingot surface to the bottom of the sump. While analogous to the flow of liquid in the thermal boundary layer along the solidification front examined by Davidson and Flood [25] and Reese [24], the current study includes the additional effect of free-floating dendrites and compositional gradients on the buoyancy force. Specific scaling coefficients are evaluated for 40 cm diameter Al–4.5 wt% Cu and Al–6.0 wt% Mg billets.

Since the billet radius and sump depth are of the same order of magnitude in DC castings [4], the billet radius, R, provides an appropriate radial and axial length scale for advection of free-floating dendrites from the billet surface to the bottom of the sump. Therefore, dimensionless coordinates are defined as $r^* = r/R$ and $z^* = z/R$, with a time scale, t_0, defined as $t_0 = R/v_0$, where t_0 represents the time required for a free-floating dendrite to be transported from the billet surface to the centerline and v_0 is the radial reference velocity such that $v^* = v/v_0$. Furthermore, a dimensionless mixture density is defined as,

$$\rho^* = \frac{\rho - \rho_l}{g_{s,p}\beta\rho_l} \tag{11}$$

where β is the solid–liquid contraction ratio, $\beta = (\rho_s - \rho_l)/\rho_l$. Since the contraction ratio, β, is less than 15% for metal systems and $g_{s,p} \leq 0.3$ in the current study, $g_{s,p}\beta \ll 1$ and $(1 + \rho^* g_{s,p}\beta) \sim 1$, and the continuity equation may be reduced to the following dimensionless form:

$$\left(\frac{\partial v^*}{\partial r^*} + \frac{v^*}{r^*}\right) + \frac{u_0}{v_0}\frac{\partial u^*}{\partial z^*} \approx 0 \tag{12}$$

suggesting comparable values for the axial and radial velocity scales, $u_0 \sim v_0$.

Reese [24] estimated thermal boundary layer velocities of approximately 60 mm/s near the solidification front while Yu and Granger [3] suggested that flow velocities in DC cast ingots may be up to two orders of magnitude higher than typical casting speeds ($\sim$100 mm/s). Accordingly, the velocity scale, v_0, of the current study is assumed to be in the range from 10 to 100 mm/s. Moreover, if a maximum characteristic diameter for an equiaxed dendrite of $d \sim 100$ μm is assumed, which is consistent with the microstructures of experimentally cast billets [1–4], Eq. (7) may be used to infer that the velocity scale, v_0, is an appropriate reference for the axial component of the solid velocity (i.e., $u_{s,0} \sim v_0$).

Dimensionless temperatures and compositions may be defined as,

$$\theta = \frac{T - T_{liq}}{\Delta T_0}, \quad F_l = \frac{f_l^A - f_0^A}{\Delta F_{l,0}}, \quad F_s = \frac{f_s^A - k_p f_0^A}{k_p \Delta F_{l,0}} \tag{13}$$

where ΔT_0 is the difference between temperatures at the liquidus ($g_s = 0$) and the interface between the slurry and mushy regions ($g_s = g_{s,p}$) for the nominal composition, f_0^A. Likewise, $\Delta F_{l,0}$ represents the difference between the liquid composition at the mushy/slurry interface ($g_s = g_{s,p}$) and the nominal composition.

Using the foregoing results and definitions, the axial slurry momentum Eq. (9) reduces to the following dimensionless form

$$\begin{aligned}
\frac{\partial u^*}{\partial t^*} + \nabla^*\left(\vec{V}^* u^*\right) \approx \frac{1}{Re_R}\Big[& \nabla^*(\nabla^* u^*) \\
& + g_{s,p}\beta\nabla^*\left(u^*\nabla^*\rho^*\right) - g_{s,p}\nabla^*\left(g_s^*\nabla^* u_s^*\right) \\
& - g_{s,p}\beta\nabla^*\left(u_s^*\nabla^* g_s^*\right) - g_{s,p}\eta_s\nabla^*\left(g_s^*\nabla^* u_s^*\right)\Big] \\
& - \nabla^*\left[\frac{g_s}{g_l}\left(\vec{V}^* - \vec{V}_s^*\right)\left(u^* - u_s^*\right)\right] \\
& + \frac{g_{s,p}}{Fr_R^2}\Big[\beta + \left(\beta_{T,l} - \beta_{T,s}\right)\Delta T_0\theta \\
& - \left(\beta_{T,l} - \beta_{T,s}\right)_0\Delta T_{SH} - \beta_{S,s}k_p\Delta F_{l,0}F_s \\
& + \beta_{S,s}\Delta F_{s,0} + \beta_{S,l}\Delta F_{l,0}F_l\Big]g_s^* \\
& - \frac{1}{Fr_R^2}\left[\beta_{T,l}\Delta T_0\theta - \beta_{T,l}\Delta T_{SH} + \beta_{S,l}\Delta F_{l,0}F_l\right] \\
& - \frac{P_{0,z}}{\rho_l v_0^2}\frac{\partial P^*}{\partial z^*}
\end{aligned} \tag{14}$$

where $Re_R = \rho_l v_0 R/\mu_l$, $Fr_R = v_0/\sqrt{Rg}$, and $P_{0,z}$, is an undetermined reference for the axial pressure gradient. In addition to the previously defined parameters, the metal superheat, $\Delta T_{SH} = T_i - T_{liq} \sim 30$ K, and the difference between the nominal composition of the liquid and the corresponding composition of the initial solid to form from liquid, $\Delta F_{s,0} = f_0^B(1 - k_p)$, appear in the buoyancy force terms. Also, the ratio of the average solid viscosity to the liquid viscosity, $\eta_s = \bar{\mu}_s/\mu_l$, is used to distinguish between solid and

liquid contributions to the viscous stress, where $\eta_s < 10$ for $g_{s,p} \leq 0.3$ [15].

The first five terms on the right side of Eq. (14) represent the combined contributions of the mixture viscous stresses to axial momentum transfer. However, since $g_{s,p}\beta \ll 1$, the second and fourth terms are negligible relative to the first term, while the first, third, and fifth terms are the same order of magnitude for $g_{s,p} \leq 0.3$. Furthermore, for aluminum-rich alloys which have liquid viscosities of approximately 0.001 kg/m s and liquid densities greater than 2300 kg/m^3 [26], $1/Re_R \ll 1$ for $10 \leq v_0 \leq 100$ mm/s. Therefore, the influence of viscous drag on the motion of liquid and free-floating dendrites along the rigid mushy zone is limited to a very thin region for which $g_s \approx g_{s,p}$, above which viscous effects have no significant influence. While viscous terms are retained in the slurry momentum equations to account for viscous effects in other regions of the sump, where they may be significant, the second and fourth terms on the right side of Eq. (9) may clearly be neglected.

The second bracketed quantity on the right side of Eq. (14), when combined with the advection term on the left side, accounts for the effects of solid and liquid phase advection. Although it increases across the slurry region, it remains less than the advection term on the left side of Eq. (14) for the range of packing fractions under consideration ($0 \leq g_{s,p} \leq 0.3$).

The third and fourth bracketed quantities on the right side of Eq. (14) consist of buoyancy force terms that account for momentum transfer due to phase density differences and density variations within each phase resulting from thermal and solutal gradients. For the aluminum alloys under consideration, liquid and solid thermal expansion coefficients, $\beta_{T,l}$ and $\beta_{T,s}$, are of the order of 10^{-4} and 10^{-5} K^{-1}, respectively, and the liquid and solid solutal expansion coefficients, $\beta_{S,l}$ and $\beta_{S,s}$, are of the order of 1. Hence, the dominant buoyancy force arises from the difference between the solid and liquid phase densities and is represented by the first term of the third bracketed quantity on the right side of Eq. (14). This term exceeds thermal buoyancy effects by at least an order of magnitude and solutal effects by at least a factor of three.

Since the advection and storage terms of Eq. (14) are of order one and the viscous terms are of order less than one, an approximate balance between the buoyancy force and the pressure gradient in the axial direction is suggested along the interface of the rigid mushy zone. This balance may be used to infer the form of the reference for the axial pressure gradient by relating the pressure coefficient to the coefficient of the dominant buoyancy term, such that $P_{0,z} \sim g_{s,p}\beta\rho_l Rg$.

As with the axial slurry momentum Eq. (9), the radial momentum Eq. (10) may be reduced to the following dimensionless form:

$$\frac{\partial v^*}{\partial t^*} + \nabla^*\left(\vec{V}^* v^*\right) \approx \frac{1}{Re_R}\left[\left(\nabla^*(\nabla^* v^*) - \frac{v^*}{(r^*)^2}\right) + g_{s,p}\beta\nabla^*\left(v^*\nabla^*\rho^*\right) - g_{s,p}\left(\nabla^*\left(g_s^*\nabla^* v^*\right) - \frac{g_s^* v^*}{(r^*)^2}\right) - g_{s,p}\beta\nabla^*\left(v^*\nabla^* g_s^*\right) + g_{s,p}\eta_s\left(\nabla^*\left(g_s^*\nabla^* v^*\right) - \frac{g_s^* v^*}{(r^*)^2}\right)\right] - \frac{P_{0,r}}{\rho_l v_0^2}\frac{\partial P^*}{\partial r^*} \quad (15)$$

Again, the third and sixth terms on the right side are negligible relative to the other viscous terms and the combined effect of the viscous terms is orders of magnitude less than that of the terms on the left side of the equation ($1/Re_R \ll 1$), suggesting that an appropriate reference for the radial pressure gradient is $P_{0,r} \sim \rho_l v_0^2$.

With respect to momentum transfer for a slurry of free-floating dendrites in DC cast billets, the foregoing scaling analysis indicates that, when viscous effects, including solid dendrite interactions, are assumed to be finite, they have little impact on overall macroscopic momentum transfer near the interface of the slurry region with the rigid mushy zone ($g_s = g_{s,p}$). One implication of this finding is that the calculation and use of an average solid viscosity will have no significant impact on the transport of free-floating dendrites from the billet surface to the bottom of the sump. The scaling analysis also indicates that the combined motion of liquid and solid in the slurry is controlled by a balance between buoyancy forces arising from mixture density variations and an adverse pressure gradient in the axial direction. Of the various mechanisms influencing the mixture density, the density difference between the solid and liquid is generally the dominant factor, with liquid composition and temperature gradients providing a second order effect.

4. Summary

The macrosegregation that occurs during the DC casting of aluminum alloys can constrain the size, alloy composition, and rate at which ingots are produced by compromising ingot quality. Experimental investigations [1–5] have shown that macrosegregation in DC cast ingots is highly dependent upon fluid flow in the melt and mushy zones, as well as in a slurry zone characterized by the transport of solute-depleted, free-floating dendrites. Furthermore, strong evidence suggests that the negative segregation commonly observed at the centerline of DC cast ingots (Fig. 1) is

caused by the transport and eventual settling of free-floating dendrites at the bottom of the sump.

To better understand and predict the complex interactions responsible for macrosegregation, a fully coupled, single-domain, mixture model of the DC casting process has been proposed. The model accounts for the redistribution of alloying elements through the transport of free-floating dendrites, as well as through fluid flow in the melt and mushy zone during solidification.

Separate and distinct mixture momentum equations are employed to account for the different momentum transfer mechanisms in two-phase regions characterized by a slurry of free-floating dendrites and a rigid, permeable dendritic matrix saturated with interdendritic liquid. A scaling analysis identified the dominant mechanisms for momentum transfer in the slurry region, which is believed to control macrosegregation at the centerline. This analysis revealed that the flow of liquid and free-floating dendrites close to the interface between the slurry and mushy regions is controlled by a balance between buoyancy forces arising from mixture density variations and an adverse pressure gradient in the axial direction.

In the companion paper [15], the model is used to predict macrosegregation distributions in Al–4.5 wt% Cu and Al–6.0 wt% Mg billets, and comparisons are made with macrosegregation trends commonly observed in DC cast ingots (Fig. 1). Furthermore, physical explanations for the manner in which various regions of segregation develop from the ingot surface to centerline are provided.

Acknowledgements

The authors would like to thank the Department of Energy for support of this research through Award Number DE-FG02-87ER13759.

References

[1] T.L. Finn, M.G. Chu, W.D. Bennon, The influence of mushy region microstructure on macrosegregation in direct chill cast aluminum–copper round ingots, in: C. Beckermann, L.A. Bertram, S.J. Pien, R.E. Smelser (Eds.), Micro/Macro Scale Phenomena in Solidification, ASME HTD, vol. 218, ASME, New York, 1992, pp. 17–26.

[2] M.G. Chu, J.E. Jacoby, Macrosegregation characteristics of commercial size aluminum alloy ingot cast by the direct chill method, in: C.M. Bickert (Ed.), Light Metals, TMS, PA, 1990, pp. 925–930.

[3] H. Yu, D.A. Granger, Macrosegregation in aluminum alloy ingot cast by the semicontinuous direct chill (DC) method, in: Aluminum Alloys: Their Physical and Mechanical Properties, EMAS, UK, 1986, pp. 17–29.

[4] R.C. Dorward, D.J. Beerntsen, Effects of casting practice on macrosegregation and microstructure of 2024 alloy billet, in: C.M. Bickert (Ed.), Light Metals, TMS, PA, 1990, pp. 919–924.

[5] B. Gariepy, Y. Caron, Investigation in the effects of casting parameters on the extent of centerline macrosegregation in DC cast sheet ingots, in: E.L. Rooy (Ed.), Light Metals, TMS, PA, 1991, pp. 961–971.

[6] B.R. Henriksen, E.K. Jensen, Modelling the effect of casting speed and metal level on the surface segregation of AA-5182, in: S.K. Das (Ed.), Light Metals, TMS, PA, 1993, pp. 969–977.

[7] A. Mo, B.R. Henriksen, E.K. Jensen, O.R. Myhr, Modelling the surface segregation development in DC casting, in: U. Mannweiler (Ed.), Light Metals, TMS, PA, 1994, pp. 889–896.

[8] E. Haug, A. Mo, H.J. Thevik, Macrosegregation near a cast surface caused by exudation and solidification shrinkage, International Journal of Heat and Mass Transfer 38 (1995) 1553–1563.

[9] P.J. Prescott, F.P. Incropera, Convection heat and mass transfer in alloy solidification, in: J.P. Hartnett, T. Irvine, Y.I. Cho, G.A. Green (Eds.), Advances in Heat Transfer, vol. 28, Academic Press, New York, 1996, pp. 231–338.

[10] C. Beckermann, C.Y. Wang, Multiphase/scale modeling of alloy solidification, in: C.L. Tien (Ed.), Annual Review of Heat Transfer VI, Begell House, New York, 1995, pp. 115–198.

[11] S.C. Flood, L. Katgerman, V.R. Voller, The calculation of macrosegregation and heat and fluid flows in the DC casting of aluminium alloys, in: M. Rappaz, M.R. Ozgu, K.W. Mahin (Eds.), Modeling of Casting, Welding and Advanced Solidification Processes V, TMS, PA, 1991, pp. 683–690.

[12] A.V. Reddy, C. Beckermann, Simulation of the effects of thermosolutal convection, shrinkage induced flow, and solid transport on macrosegregation and equiaxed grain size distribution in a DC continuous cast Al–Cu round ingot, in: V.R. Voller, S.P. Marsh, N. El-Kaddah (Eds.), Materials Processing in the Computer Age II, 1995, pp. 89–102.

[13] J. Ni, C. Beckermann, A volume-averaged two-phase model for transport phenomena during solidification, Metallurgical and Materials Transactions B 22B (1991) 349–361.

[14] A.V. Reddy, C. Beckermann, Modeling of macrosegregation due to thermosolutal convection and contraction-driven flow in direct chill continuous casting of an Al–Cu round ingot, Metallurgical and Materials Transactions B 28B (1997) 479–489.

[15] C.J. Vreeman, F.P. Incropera, The effect of free-floating dendrites and convection on macrosegregation in direct chill cast aluminum alloys Part II: predictions for Al–Cu and Al–Mg alloys, International Journal of Heat and Mass Transfer 43 (2000).

[16] W.D. Bennon, F.P. Incropera, A continuum model for momentum, heat and species transport in binary solid–liquid phase change systems — I. Model formulation,

International Journal of Heat and Mass Transfer 30 (1987) 2161–2170.
[17] P.J. Prescott, F.P. Incropera, W.D. Bennon, Modeling of dendritic solidification systems: reassessment of the continuum momentum equation, International Journal of Heat and Mass Transfer 34 (1991) 2351–2358.
[18] J. Ni, F.P. Incropera, Extension of the continuum model for transport phenomena occurring during metal alloy solidification — I. The conservation equations, International Journal of Heat and Mass Transfer 38 (1995) 1271–1284.
[19] J. Ni, F.P. Incropera, Extension of the continuum model for transport phenomena occurring during metal alloy solidification — II. Microscopic considerations, International Journal of Heat and Mass Transfer 38 (1995) 1285–1296.
[20] M. Ishii, N. Zuber, Drag coefficient and relative velocity in bubbly, droplet or particulate flows, American Institute of Chemical Engineers Journal 25 (1979) 843–855.
[21] W.D. Bennon, F.P. Incropera, A continuum model for momentum, heat and species transport in binary solid–liquid phase change systems — II. Application to solidification in a rectangular cavity, International Journal of Heat and Mass Transfer 30 (1987) 2171–2187.
[22] W.D. Bennon, F.P. Incropera, Numerical analysis of binary solid–liquid phase change using a continuum model, Numerical Heat Transfer 13 (1988) 277–296.
[23] M.J.M. Krane, F.P. Incropera, A scaling analysis of the unidirectional solidification of a binary alloy, International Journal of Heat and Mass Transfer 39 (1996) 3567–3579.
[24] J.M. Reese, Characterization of the flow in the molten metal sump during direct chill aluminum casting, Metallurgical and Materials Transactions B 28B (1997) 491–499.
[25] P.A. Davidson, S.C. Flood, Natural convection in an aluminum ingot: a mathematical model, Metallurgical and Materials Transactions B 25B (1994) 293–302.
[26] E.A. Barnes, G.B. Brook (Eds.), Smithell's Metals Reference Handbook, 7th ed., Butterworth–Heinemann, Oxford, 1992, pp. 1406–1408.